Luminescent Gold Nanocluster-Methylcellulose Composite Optical Fibers with Low Attenuation Coefficient and High Photostability

Ville Hynninen, Sourov Chandra, Susobhan Das, Mohammad Amini, Yunyun Dai, Sakari Lepikko, Pezhman Mohammadi, Sami Hietala, Robin H. A. Ras, Zhipei Sun, Olli Ikkala, Nonappa**

V. Hynninen, Prof. Nonappa
Faculty of Engineering and Natural Sciences, Tampere University
P.O. Box 541, FI-33101 Tampere, Finland
E-mail: nonappa@tuni.fi

V. Hynninen, Dr. S. Chandra, S. Lepikko, Prof. R. H. A. Ras, Prof. O. Ikkala, Prof. Nonappa
HYBER Centre of Excellence, Department of Applied Physics
Aalto University, P. O. Box 15100, FI-00076, Espoo, Finland
E-mail: olli.ikkala@aalto.fi

Dr. S. Das, M. Amini, Dr. Y. Dai, Prof. Z. Sun
Department of Electronics and Nanoengineering, Aalto University
Tietotie 3, FI-02150, Espoo, Finland

Dr. S. Das, M. Amini, Dr. Y. Dai, Prof. Z. Sun
QTF Centre of Excellence, Department of Applied Physics, Aalto University, FI-00076, Espoo, Finland

Dr. P. Mohammadi
VTT Technical Research Centre, P.O. Box 1000, FI-02044, Espoo, Finland

Dr. S. Hietala
Department of Chemistry, University of Helsinki P.O. Box 55, FI-00014, Helsinki, Finland.

Keywords: methylcellulose, gold nanoclusters, cellulose nanocrystal, biopolymer, nanocomposites, optical fibers, photoluminescence

Abstract:

Because of their lightweight structure, flexibility, and immunity to electromagnetic interference, polymer optical fibers (POFs) have been used in numerous short-distance applications. Notably, the incorporation of luminescent nanomaterials in POFs offers optical amplification for advanced nanophotonics. However, conventional POFs suffer from non-sustainable components and processes. Furthermore, the traditionally used luminescent nanomaterials undergo photobleaching, oxidation and can be cytotoxic. Therefore, biopolymer-based optical fibers containing non-toxic luminescent nanomaterials are needed, with efficient

and environmentally acceptable extrusion methods. Here, we demonstrate such an approach for fibers wet-spun from aqueous methylcellulose (MC) dispersions under ambient conditions. Further, the addition of either luminescent gold nanoclusters, rod-like cellulose nanocrystals, or gold nanocluster-cellulose nanocrystal hybrids into the MC matrix furnished strong and ductile composite fibers. Using cutback attenuation measurement, we show that the resulting fibers can act as short-distance optical fibers with propagation loss as low as 1.47 dB cm^{-1}. The optical performance is on par with or even better than some of the previously reported biopolymeric optical fibers. The combination of excellent mechanical properties (Young´s modulus and maximum strain values up to 8.4 GPa and 52%, respectively), low attenuation coefficient and high photostability makes the MC-based composite fibers excellent candidates for multifunctional optical fibers and sensors.

1. Introduction

Optical fibers are the current mainstream choice for fast and high-capacity communication networks.[1] The state-of-the-art silica glass optical fibers (GOFs) have an attenuation coefficient of ca. 0.2 dB km^{-1}, i.e., they can carry signals over tens of kilometers without significant losses or need for amplification.[2] However, they are not optimal for certain short-distance optical fiber technologies such as selected automotive, household networks, smart textiles, and biosensors due to their brittleness, lack of flexibility, poor modifiability, and limited biocompatibility.[3] By contrast, polymeric optical fibers, aka plastic optical fibers (POFs), have the potential to overcome such limitations. They are cost-effective and offer mechanical softness and ductility.[4] The synthetic POFs typically consist of a high refractive index (RI) poly (methyl methacrylate) (PMMA, RI ~1.49), or polystyrene (PS, RI ~1.56) core surrounded by a low refractive index fluorinated polymer (RI ~1.35) cladding. They can also incorporate functional dopants in their matrix,[5–8] such as dye molecules (e.g., rhodamine B, rhodamine 6G, and perylene),[9] noble metal nanoparticles,[10] quantum dots,[11] and rare earth

metal ions,[12] for optical amplification and nanophotonic applications. Nanoparticle doped composite fibers have been utilized as sensors,[13] wearable and stretchable devices,[14] and for inactivation of bacteria.[15] However, most of the existing luminescent dye molecules and nanomaterials are prone to photobleaching, oxidation and can be cytotoxic.[16-20] The POFs have inherently higher attenuation coefficients (0.16 dB m^{-1} to 0.30 dB m^{-1}) than those of GOFs.[7,21] Nevertheless, the attenuation coefficient of POFs is sufficient for short length scale applications. To fully exploit the POF potential, there have been challenges due to environmental aspects such as high-temperature processing, toxic/hazardous chemical treatments, and limited biodegradability.[22–24] To overcome such limitations, synthetic biocompatible polymers and biopolymer-based fibers have been studied in the literature for their light propagation properties.

Biopolymers, such as agarose and alginate-based hydrogels,[25–28] gelatin,[29,30] chitosan,[31-33] silk,[34–38] and DNA,[39,40] allow optical waveguides. Cellulose is a renewable and sustainable polymer with RI ~ 1.51 - 1.47, depending on the derivatization. Surprisingly, it has not been broadly explored for fiber optics,[41] even though various cellulose derivatives and nanocelluloses have been widely studied for several other photonic applications.[42-54] Among a few examples, cellulose-derived optical fibers have been reported based on hydroxypropyl cellulose (core)-cellulose butyrate (cladding) fibers and cellulose acetate -coated regenerated cellulose fibers.[55,56] Their preparation still involves high temperature treatments and ionic liquids. Methylcellulose (MC) is a well-known charge-neutral polymer (RI ~ 1.49) studied as a potential alternative for oil-based polymers for, e.g., foods, detergents, paints, adhesives, cosmetics, pharmaceuticals, and functional gels.[57–59] MC is a water-dispersible polymer that shows lower critical solution temperature (LCST) behavior, i.e., it forms turbid hydrogels at elevated temperatures (**Figure 1a**).[60–62] Upon gelation, MC chains self-assemble into fibrillar bundles and increase the gel stiffness. The mechanical properties of the MC polymer network can be altered by adding nanoparticles, such as cellulose nanocrystals (CNCs) or chitin

nanocrystals offering a facile route for composite nanomaterials.[59–61] Moreover, cellulose-gold nanoparticle composites have been studied for their catalytic performance, sensing and optoelectronic properties.[63] Among gold nanoparticles, atomically precise gold nanoclusters (Au NCs) have recently gained considerable attention due to their well-defined molecular structure, photostability, non-toxicity, and biocompatibility.[64-69] Their small size, water solubility, and molecule-like optoelectronic properties allow dispersion in hydrogels.[70] Gold nanoclusters also possess a high surface-to-volume ratio, excellent catalytic effect, and they enable sensing of heavy metal ions.[64-70] Among Au NCs, bovine serum albumin (BSA) coated gold nanoclusters (Au@BSA) and reduced glutathione (GSH) capped gold nanoclusters (Au@GSH) have been explored for sensors, catalysis, bioimaging, and pathogen detection.[71-83] However, their potential in biopolymer-based composite fibers for optical amplification and waveguiding is unexplored to date.

Here we use aqueous MC dispersions and MC-nanoparticle composite hydrogels to wet-spin fibers under ambient conditions without any hazardous chemicals or treatment. Therein, four types of dopants (nanoscale additives) were used, *viz*., (i) bovine serum albumin encapsulated gold nanocluster (Au@BSA), (ii) glutathione capped gold nanoclusters (Au@GSH), (iii) (i) sulfuric acid hydrolyzed cellulose nanocrystals (CNCs), and (iv) Au@GSH covalently linked to cellulose nanocrystals (CNC-Au@GSH). We demonstrate the effect of hydrogel solid content and dopants on the fiber mechanical, optical, and attenuation properties. Finally, we show that the fiber-embedded gold nanoclusters retain their intrinsic optoelectronic and metal ion sensing properties with enhanced photostability under continuous ultraviolet (UV) light irradiation. We also show temperature-dependent degradation in an aqueous environment.

2. Results and Discussion

2.1 Preparation and Characterization of Gold Nanoclusters, Cellulose Nanocrystals, and Their Hybrids

Figure 1 summarizes the components used to prepare MC-based nanocomposite optical fibers with Au NCs, CNCs, and their hybrids. For the fiber matrix, the aqueous dispersions of commercial MC polymer (MW 88000 g/mol, degree of substitution 1.5-1.9) were prepared according to reported procedures (Figure 1a).[84,85] The system to spin fibers from aqueous dispersions and hydrogels is shown schematically in Figure 1b. For the optical functionalities, the synthesis of luminescent gold nanoclusters Au@BSA and Au@GSH was carried out using $HAuCl_4.3H_2O$ in the presence of BSA and GSH ligands, respectively (Figure 1c-h).[76] For the reinforcement and templating of gold nanoclusters, CNCs were prepared by sulfuric acid hydrolysis with an average length of 238 nm and an aspect ratio of ca. 14 with sulfate half ester content of 239 μmol g^{-1} (Figures 1i, j, **Figure S1**, Supporting Information).[84,85] To prepare glutathione capped gold nanocluster hybrids with cellulose nanocrystals (CNC-Au@GSH), the precursor ($HAuCl_4.3H_2O$) was bound onto aqueous CNCs followed by the addition of GSH ligands. The TEM image of CNC-Au@GSH displayed an inter-nanocluster distance of ~ 5 nm over the CNC surface (Figure 1k).

The presence of Au, C, O, and two different types of S atoms in CNC-Au@GSHs was confirmed using energy dispersive X-ray (EDX) and X-ray photoelectron spectroscopy (XPS) analysis (**Figures S**2 and **S**3, Supporting Information). The XPS spectrum corresponding to S2p3/2 appeared as a single peak at 169.2 eV for CNCs (**Figure S**3b, Supporting Information). However, an additional peak at a lower oxidation state at around 163.1 eV was also observed in CNC-Au@GSH due to the presence of (i) the $-OSO_3^-$ groups in CNCs and (ii) -SH groups of GSH. The Au4f7/2 XPS spectrum of CNC-Au@GSH confirmed typical peak positions of gold nanoclusters with Au(0) core and Au(I) surfaces at 83.9 eV and 84.8 eV, respectively (Figure S3c, Supporting Information).[76]

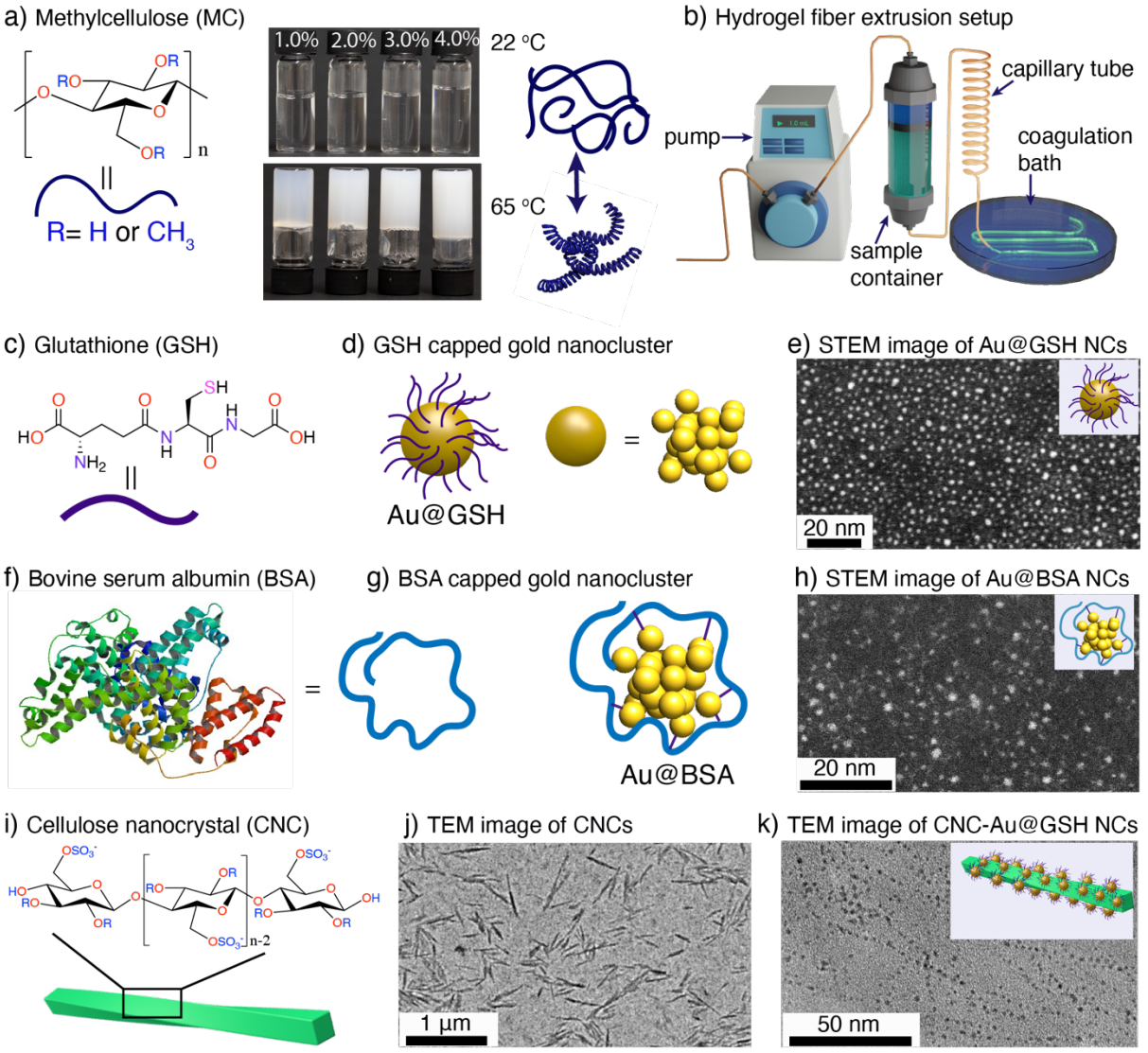

Figure 1. Materials and methods used in this study. a) The chemical structure of MC, scheme of its aq. conformations, and photographs of 1, 2, 3, and 4 w/v% aq. solutions at 22 °C (viscous fluids, top) and 65 °C (gels, bottom). b) Schematic of the fiber extrusion setup. c) Chemical structure of glutathione (GSH). d) Schematic showing GSH capped gold nanoclusters (Au@GSH NCs). e) Darkfield (DF) STEM image of Au@GSH NCs. f) The structure of bovine serum albumin (BSA, PDB ID 3VO3). g) Schematic representation of BSA capped gold nanocluster (Au@BSA). h) DF STEM image of Au@BSA. i) Chemical structure and schematic representation of cellulose nanocrystal (CNC). j) TEM of image CNCs. k) TEM image of CNC-Au@GSH (inset shows the schematic of CNC-Au@GSH).

The aqueous dispersions of gold nanoclusters Au@BSA and Au@GSH showed the characteristic absorption peaks at 520 nm and 400 nm, respectively, in UV-vis absorbance spectra (**Figure 2**a, see the experimental section for details). However, in the CNC-Au@GSH hybrid, i.e., upon templating Au@GSH on CNC, they could not be resolved, presumably due to the high CNC content compared to that of Au@GSH (~2.6%) and their overlapping

absorptions. The photoluminescence excitation (PLE) spectrum at 600 nm emission showed a broad peak centered around 390 nm for both Au@GSH and CNC-Au@GSH (Figure 2b). This suggests that in CNC-Au@GSHs, the optical properties of Au@GSH were well retained after binding on CNCs. The PL emission spectra of Au@BSA and Au@GSH showed broad peaks centered at 660 nm (at λ_{ex} = 470 nm) and 590 nm (at λ_{ex} = 400 nm), respectively (Figure 2c). Importantly, for CNC-Au@GSHs, the position of PL emission peak corresponding to Au@GSH was unaltered upon chemically binding with CNCs (Figure 2c), and it showed a strong fluorescence under UV-irradiation (Figure 2d).

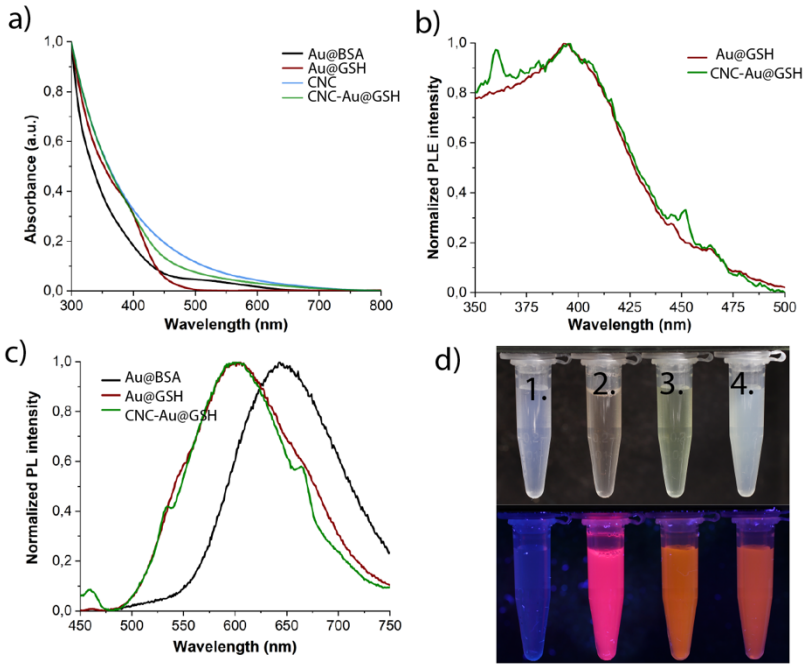

Figure 2. Optical properties. a) UV-vis absorption spectra of Au@BSA, Au@GSH, CNC, and CNC-Au@GSH aq. dispersions. b) Photoluminescence excitation spectra of free Au@GSH and CNC-Au@GSH. c) Photoluminescence emission spectra of Au@BSA, Au@GSH, and CNC-Au@GSH. d) Photographs at ambient conditions (above) and under UV light (below): 1) 1.0% CNCs, 2) 1.0% Au@BSA, 3) 0.04% Au@GSH, 4) 1.0% CNC-Au@GSH.

2.2 Rheological Properties of MC and Composite Hydrogels

The strain sweeps, frequency sweeps, and the shear viscosities of the MC aqueous dispersions and the composites were determined using oscillatory rheology at 22 °C (**Figure 3**). The strain sweep experiments of pure MC aqueous dispersions (2.0 - 4.0%, note: all % refers to weight of the solid/volume of the solvent %) displayed loss moduli (*G´´)* higher than storage moduli (*G´*),

thus suggesting viscous flow (Figure 3a). *G′* increased considerably with increasing MC concentration, i.e., showing values of 7, 43, and 154 Pa for 2.0, 3.0, and 4.0%, respectively. Notably, in the frequency sweep experiments, the *G′* and *G′′* slopes *vs*. frequency are roughly equal for a given composition, thus suggesting that they are, in fact, close to sol-gel transition state 22 °C (Figure 3b). The viscosity increased as a function of MC solid content from 8, 25 to 105 Pa.s for 2.0, 3.0, and 4.0% MC, respectively (Figure 3c). Shear thinning at 22 °C was observed for all compositions, which is beneficial for wet-spinning.

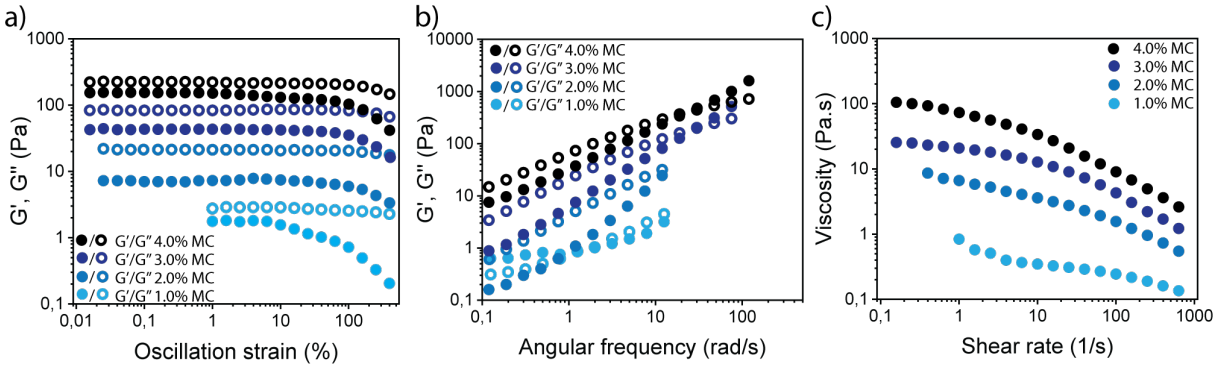

Figure 3. Rheological characterization of MC aqueous dispersions at 22 °C. a) Strain sweeps, b) frequency sweeps, and c) steady-shear flow sweeps of 1.0, 2.0, 3.0, and 4.0% MC aqueous dispersions.

In rheological measurements, the MC/Au@BSA and MC/Au@GSH composites displayed liquid-like behavior at all the studied compositions (Figure 4). However, MC/CNC-Au@GSH, MC/CNC, and a three-component mixture of MC/CNC/Au@BSA all displayed *G′* > *G′′*, indirectly suggesting more gel-like rheological properties (Figure 4). The *G′* of MC/Au@BSA for 3.0%/0.75% (note: all %s refers to the weight of the solid/volume of the solvent %) was slightly higher (52 Pa) than that of pure MC 3.0%, presumably due to an increase in the solid content. However, for MC/Au@BSA 3.0%/1.0% (i.e., the overall solid content of 4.0%), the *G′* was similar to that of the 3.0%/0.75% composition. This suggests limited mechanical reinforcement of composite gels by Au@BSAs.

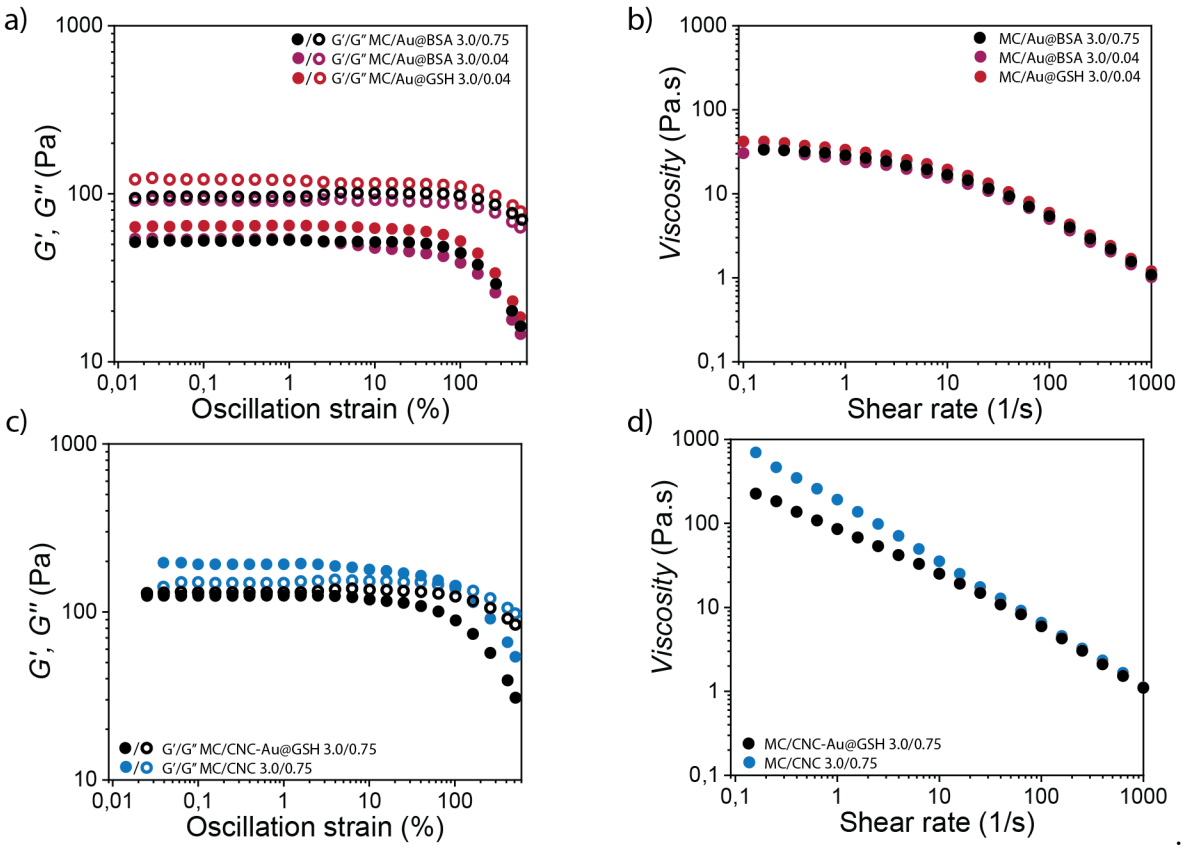

Figure 4. Rheological properties of MC nanocomposite dispersions and hydrogels. a,b) Strain and shear sweeps of aq. MC/Au@BSA and MC/Au@GSH composites. c,d) Strain and shear sweeps of MC/CNC and MC/CNC-Au@GSH composite hydrogels.

Furthermore, keeping the overall solid content identical (i.e., 4.0%) but altering the weight ratio of MC to Au@BSA from 3:1 to either 2:2 or 1.4:2.6 further reduced the hydrogel modulus. This suggests that 3.0% MC is a feasible concentration. Therefore, the amount of gold nanoclusters that maintains the mechanical properties of the composites close to that of 3.0% MC were optimized. For example, MC/Au@BSA 3.0%/0.04% composition displayed G' of 41 Pa and the viscosity of 34 Pa.s, which are close to those of pure 3.0% MC. Similar experiments with the MC/Au@GSH 3.0%/0.04% composition showed slightly higher storage modulus (64 Pa) and viscosity (54 Pa.s). Interestingly, such a low loading of gold nanoclusters was enough to impart luminescence to the composite systems.

The composition MC/CNC-Au@GSH 3.0%/0.75% displayed near gel-like properties ($G' \approx G''$) with a G' value of 125 Pa (Figure 4c, d). In comparison, MC/CNC 3.0%/0.75% showed G' of 194 Pa and viscosity of 622 Pa.s indicative of significant stiffening accompanied with more gel-like characteristics (i.e., $G' > G''$) and frequency-independent G' scaling (Figure 4c, d and **Figure S**7, Supporting Information). A second control sample containing MC/BSA 3.0%/0.75% displayed higher G' and viscosity (68 Pa and 56 Pa.s, respectively) compared to the MC/Au@BSA 3.0%/0.75% (**Figures S**4 and **S**5, Supporting Information). This is expected since, under gold nanocluster synthesis conditions, BSA ligands undergo structural changes compared to native BSA. Finally, a three-component control system with a composition of MC/CNC/Au@BSA 3.0%/0.73%/0.02% behaved similarly to MC/CNC 3.0%/0.75% control in its rheological behavior (**Figures S**4 and **S**5, Supporting Information). In the literature, highly elongated anisotropic nanofillers have been demonstrated to yield higher mechanical reinforcement than smaller aspect ratio spherical particles. Our results are in line with the existing literature on CNC reinforced composite hydrogels.[86]

2.3 Fiber Spinning and Morphology

MC aqueous dispersion and the composite hydrogels were wet-spun into solid fibers by extrusion through a capillary tube (ø = 1 mm, length = 1 m) into a coagulation bath filled with ethanol (96.0 v/v%) at 22 °C (Figure 1b, see Experimental section for details).[85,86] The resulting fibers were structurally uniform, smooth and transparent (Figure 5). However, due to relatively low overall solid content, the gravity-driven flattening during the coagulation resulted in fibers with non-cylindrical and folded cross-sections (Figure 5e, f and Figures S8 and S9**,** Supporting Information). The pure MC-based fibers were highly transparent with a glass-like appearance. The addition of dopants slightly altered the appearance and transparency of the fibers. MC/Au@BSA fibers displayed a pale reddish hue at low Au@BSA concentration but turned red and opaque at higher concentrations (Figure 5 and **Figure S10,** Supporting

Information). MC/Au@GSH and MC/CNC-Au@GSH compositions produced yellowish and non-transparent fibers. Importantly, nanocomposite fibers with sufficient gold nanocluster loadings displayed luminescence under UV irradiation (Figures 5c, d and Figure S10, Supporting Information). The SEM images of fractured fiber cross-sections showed oriented assemblies of rod-like internal structures to radiate from the fiber core towards the edges (Figure 5g and Figure S11, Supporting Information). The rod-like nanostructures have been earlier proposed to consist of hybrids of MC and CNCs in MC/CNC fibers.[81] Here, the nanostructures were also observed in pure MC fibers, showing that they inherently stem from the MC component.

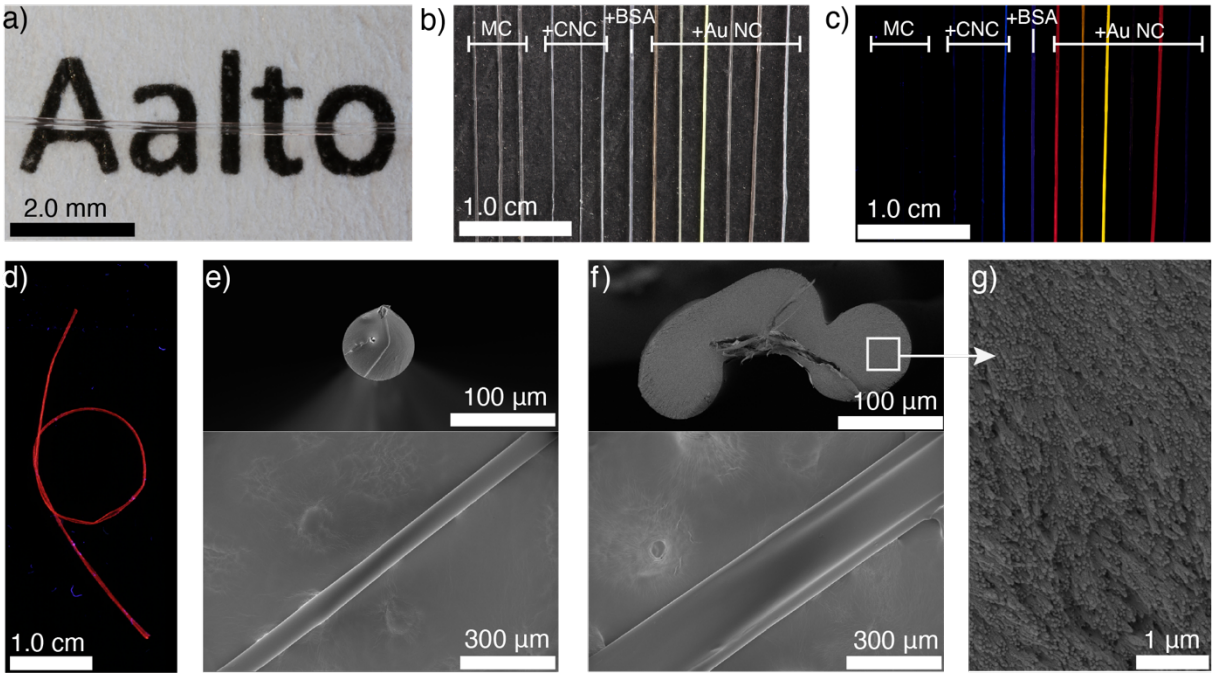

Figure 5. Morphology of MC-based composite fibers. a) Photograph showing a highly transparent fiber on a printed text spun from 3.0% MC dispersion, b) Photographs of composite fibers (from left to right: MC 2.0, MC 3.0, MC 4.0, MC/CNC 1.0/0.25, MC/CNC 2.0/0.50, MC/CNC 3.0/0.75, MC/BSA 3.0/0.75, MC/Au@BSA 3.0/075, MC/CNC-Au@GSH 3.0/0.75, MC/Au@GSH 3.0/0.04, MC/Au@BSA 3.0/0.04, MC/CNC-Au@BSA 3.0/0.375/0.37, and MC/CNC-Au@BSA 3.0/0.73/0.02. c) The same fibers as in (b) photographed under UV light. d) MC/Au@BSA 3.0/0.75 fiber shows intense photoluminescence under UV light and allows significant bending without breaking. e) SEM images of the fractured cross-section and side view of and MC 2.0 fiber. f) SEM images of the fractured cross-section and side view of and MC 4.0 fiber. g) High magnification SEM image of the MC 4.0 fiber cross-sectional surface showing rod-like internal features.

2.4 Fiber Mechanical Performance

Uniaxial tensile tests were performed to determine the mechanical properties of the wet-spun fibers. The fibers are henceforth denoted by their initial aq. dispersion, for example MC 2.0 has been spun from 2.0% MC aq. dispersion. Typical average mechanical properties (maximum stress, maximum strain, Young's modulus, and modulus of toughness) for selected fiber compositions are given in Table 1 (see Table S1, Supporting Information, for further mechanical data). Pure MC fibers showed an increasing maximum strength and stiffness with increasing total solid content (Figure 6a). For example, an average maximum strength of 97.1, 109.4, and 151.7 MPa were observed for MC 2.0, MC 3.0, and MC 4.0 fibers, respectively. However, at the same time, the maximum strain decreased from 52.4% to 32.2% for fiber spun from aq. 2.0 to 4.0% solution. The modulus of toughness remained rather constant regardless of the MC content. Overall, MC 2.0 fibers achieved the highest maximum strain (52.4%) of all the tested compositions, and it can be considered significantly high for a cellulose-based fiber.[90] The low MC content was deduced to allow low-density looser packing, which enabled enhanced ductility. In contrast, higher MC content became more densely packed, resulting in high stiffness but reduced flexibility.

Table 1. Representative mechanical properties of selected MC and composite fibers.

Fiber composition	Max stress [MPa]	Max strain [%]	Young's modulus [GPa]	Modulus of toughness [MJ m^{-3}]
MC 3.0	109.4 ± 56.9	47.6 ± 16.5	2.6 ± 1.2	31.8 ± 18.7
MC 4.0	151.7 ± 33.0	32.2 ± 7.3	4.0 ± 0.4	31.5 ± 11.5
MC/Au@BSA 3.0/0.75	127.6 ± 15.9	34.9 ± 7.8	4.0 ± 0.4	29.9 ± 9.3
MC/BSA 3.0/0.75	126.8 ± 28.6	35.6 ± 5.1	3.4 ± 0.7	29.5 ± 9.5
MC/Au@BSA 3.0/0.04	160.0 ± 33.5	34.1 ± 7.5	4.1 ± 0.4	35.8 ± 13.1
MC/Au@GSH 3.0/0.04	161.9 ± 27.7	45.1 ± 11.4	4.1 ± 0.3	48.9 ± 17.8
MC/CNCAu@GSH 3.0/0.75	161.6 ± 14.9	43.8 ± 6.9	5.4 ± 0.5	47.8 ± 10.1
MC/CNC/Au@BSA 3.0/0.73/0.02	173.4 ± 24.9	43.4 ± 6.3	6.1 ± 0.5	52 ± 12.2
MC/CNC/Au@BSA 3.0/0.375/0.375	154.8 ± 26.5	37.5 ± 9.8	5.0 ± 0.8	38.8 ± 14.9
MC/CNC 3.0/0.75	173.0 ± 19.5	33.8 ± 6.4	8.3 ± 1.1	41.4 ± 10.0

The mechanical properties of MC/Au@BSA 3.0/0.75 fibers were expectedly between those of MC 3.0 and MC 4.0 fibers (Table 1 and Figure 6b), but stronger than those of the MC/BSA 3.0/0.75 control fibers (Figure 6c). This suggests that Au@BSAs provide better reinforcement to the composite fibers in their dried state than free BSA protein. This is attributed to the fact that in the Au@BSA, their rigid metal core could efficiently induce semi-stiff surrounding interfacial regions and contribute to the overall material stiffness compared to the liquid-state.[87-89] Furthermore, adjusting the MC to Au@BSA ratio more towards the Au@BSA resulted in weaker, softer, and more ductile fibers, which is in agreement with their rheological behavior of the corresponding composition in solution state (Figure S12**,** Supporting Information).

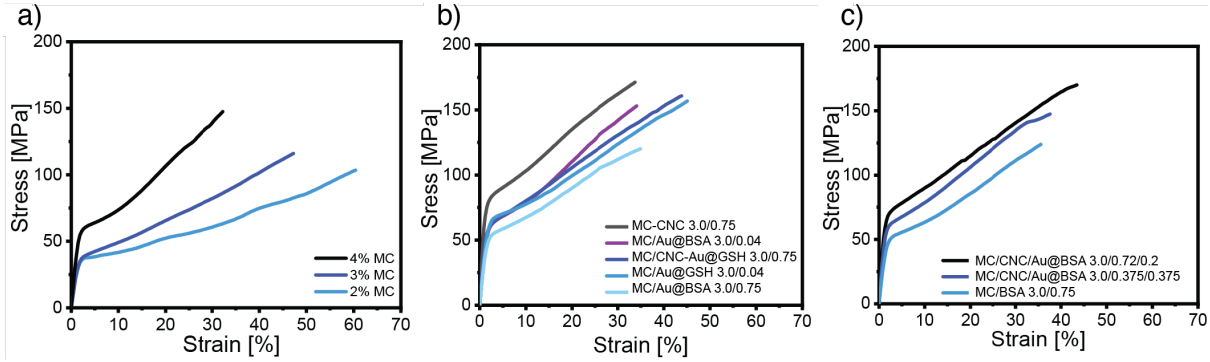

Figure 6. Tensile test performance of MC and composite based fibers. a) Representative stress-strain curves of pure MC fibers. b) Stress-strain curves of MC/Au@BSA, MC/Au@GSH, MC/CNC, and MC/CNC-Au@GSH composite fibers. c) Stress-strain curves of MC/BSA and the three-component MC/CNC/Au@BSA composite fibers.

Surprisingly, the composite fibers with very low Au@BSA and Au@GSH loadings of 0.04% outperformed the pure MC 4.0 fibers in all mechanical aspects regardless of their ~25% lower overall solid content (Table 1). This suggests that the mechanical benefits of the Au NCs also in dry composites are best exploited at minimal loadings. However, 0.04% Au@BSA loading was not sufficient to impart luminescence to the composite fibers. On the other hand, 0.04% Au@GSH doped fibers were strongly fluorescent but turned opaque. The observed difference between the two types of gold nanocluster-doped fibers is presumably due to the different ligand coatings. Similarly, MC/CNC-Au@GSH 3.0/0.75 fibers surpassed the mechanical properties of MC 4.0 fibers but were optically not transparent. The denser material in the dried solid state is suggested to enable CNC-Au@GSHs to more tightly interact with the surrounding MC matrix and take advantage of the rigidness of the CNC-Au@GSH hybrids. However, again the CNC-Au@GSH additive fiber reinforcement (162 MPa maximum stress, 4.1 GPa Young's modulus) remained lower compared to pure CNCs (173 MPa maximum stress, 8.3 GPa Young´s modulus), even though it allowed slightly more ductile (43.8% maximum strain) fibers (Table 1). Importantly, a balance between the optimal mechanical performance available through CNCs and luminescence of the Au NCs could be achieved by adding a low weight fraction of Au@BSA to MC/CNC composite hydrogels. Accordingly, a three-component system containing MC/CNC-Au@BSA of 3.0%/0.375%/0.375% allowed

luminescent fibers with good mechanical properties (155 MPa ultimate stress, 37.5% maximum strain, 5.0 GPa Young's modulus) close to those of MC/CNC fibers (Table 1, Figure 6c). The performance of various MC-based fibers was generally approximately on par or better than other known cellulose-based optical fibers.[55,56]

2.5 Optical Fiber Performance

The total internal reflection (TIR) phenomenon that traps the light signals within optical fibers and guarantees efficient signal transmission requires a surrounding medium (cladding) with lower RI than the fiber core. Typically, in commercial optical fibers, this is ensured by a separate cladding layer on top of the core fiber. Here the MC fibers were prepared and manipulated as uniform refractive index core-only, i.e., their optical fiber performance directly relies on the relative optical characteristics of their surroundings. Refractive indices of the MC and MC nanocomposites were determined from spin-coated thin films using ellipsometry (Figures S13 and S14**,** Supporting Information). The refractive indices of the MC-based nanocomposites were in the range of ~1.48-1.50 (at λ = 632.8 nm), depending on the nanodopant type and concentration. Typically, pure nanodopants displayed higher RI, e.g., 1.51 for Au@BSA and 1.56 for CNCs, due to their high crystallinity compared to amorphous and less dense pure MC (RI ~1.48). As a result, the refractive indices of the nanocomposites gained intermediate values. For instance, the addition of CNC-Au@GSHs or CNCs to MC increased the observed RI from 1.48 of pure MC up to ~1.50 in the mixtures. Instead, the addition of Au@BSA and Au@GSH gave only a minor increase in RI compared to pure MC since their densely packed cores occupy significantly smaller volumes compared to CNCs and, thus, contribute less to the overall density of the nanocomposites.

Finally, representative samples of each fiber composition were studied for their potential for optical fiber and signal transmission efficiency.

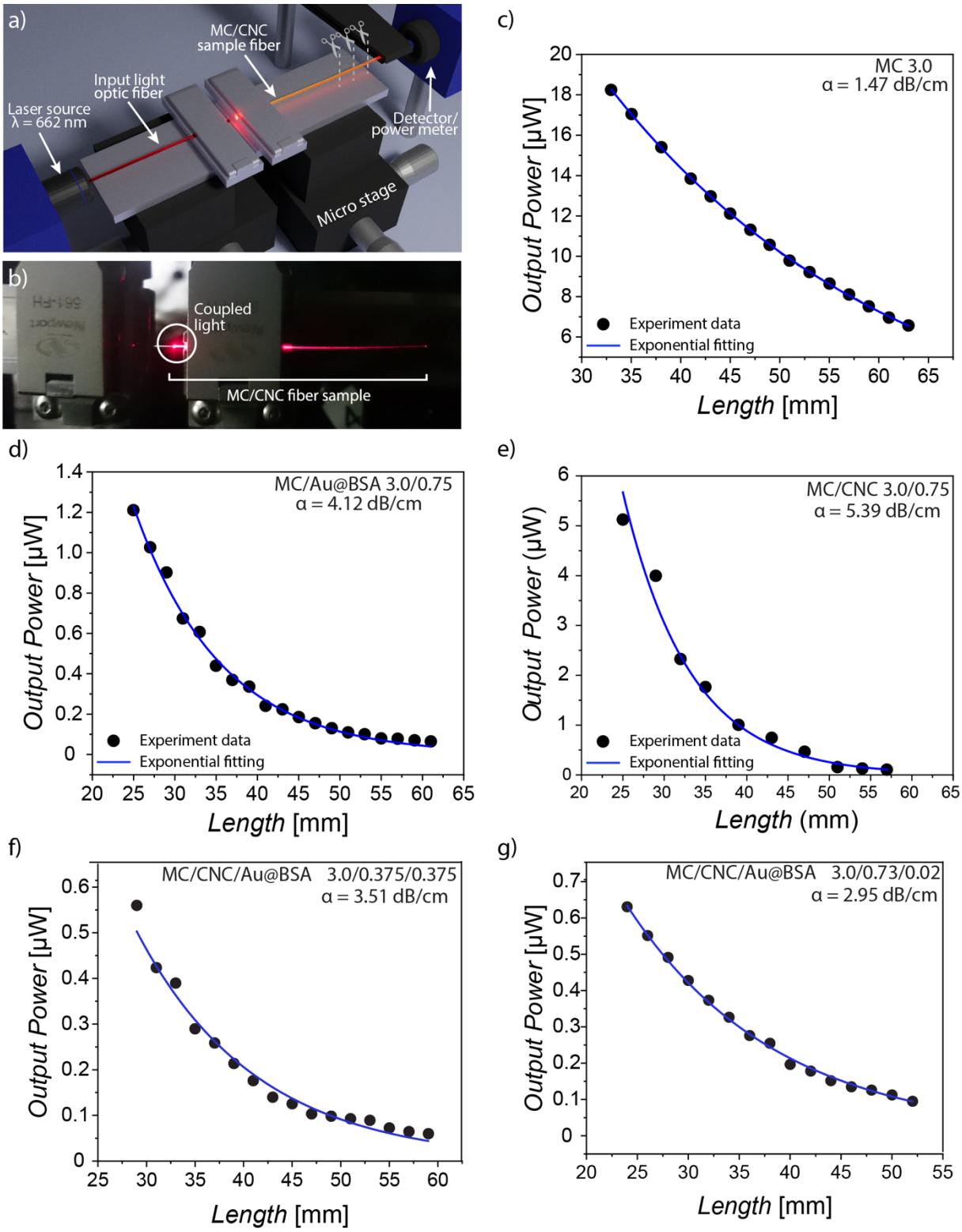

Figure 7. Attenuation coefficients of MC and composite optical fibers. a) Schematic drawing of the cutback measurement setup. Light is coupled to the sample fibers and output light intensity is measured repeatedly at different fiber lengths. b) Photograph of the coupled light propagating inside an MC/CNC 2.0/0.50 optical fiber sample during the cutback experiment. c-e) Representative experimental cutback data (black circles) and experimental fitting (solid blue line) of MC 3.0, MC/Au@BSA and MC/CNC composite fibers.

For the ease of manipulating and efficiently coupling the light into the fibers, compositions that produced thicker fibers were preferably selected, whenever possible. The fibers' ability to transmit light signals was determined by measuring the attenuation coefficients (α) of each fiber type with a cutback method using a continuous-wave red laser (λ = 662 nm) (Figure 7 and Figures S15-S16, Supporting Information). Therein, a light signal with a known intensity was shone into the fiber from one end and the output power at different propagating lengths along the fiber was measured. Thus, the power of the output light at different fiber lengths was measured and the attenuation coefficients (α) were determined from the experimental data through a mathematical fitting. For materials with attenuation coefficient (α), the output intensity *I(z)* can be described with Beer-Lambert law (equation 1):

$$I(z) = I(0)e^{-\alpha z} \quad (1)$$

Where *z* is the propagating length of the light along the fiber, *I(0)* the input light power, and *I(z)* the light power at different *z*. The experimentally determined attenuation coefficients (α) allowed quantitative comparison of the nanocomposites as optical fibers and the evaluation of the effects of each dopant similar to mechanical properties.

Clear and glass-like pure MC 3.0 and MC 4.0 allowed excellent wave propagation with attenuation coefficient α of 1.47 dB cm^{-1} and 2.64 dB cm^{-1}. Even though the MC fiber performance is abysmal compared to the state-of-the-art commercial silica optical fibers designed for long-range communication (~0.2 dB km^{-1}), the attenuation coefficient of 1.47 dB cm^{-1} is on par or better than many biopolymer-based optical fibers reported in the literature.[56] It is important to note that the fibers studied in this work have no cladding layer (i.e., the surrounding air acts as a cladding). For instance, α of the relatively well-studied and well-performing silk optical waveguides generally fall in the range of 0.25-10.5 dB cm^{-1} depending on the waveguide type and environment.[27–36,57,58]

MC/Au@BSA 3.0/0.75 fibers were found relatively efficient as optical fibers with α of 4.12 dB cm^{-1}, which was only slightly higher than that of MC 4.0 fibers. Thus, regardless of the addition of gold, the optical fiber capabilities were rather well retained. However, good-quality fibers were essential for optical fiber performance. It was observed that any significant defects, such as small fiber-trapped air bubbles or impurities, easily resulted in highly absorbing hot spots that suppressed the propagating signals. The performance of MC/Au@BSA was also compared against MC/BSA 3.0/0.75 control fiber with α = 4.21 dB cm^{-1} to further elucidate the role of gold. Based on the attenuation coefficients, the Au@BSA did not significantly enhance absorption than pure BSA protein of similar weight fraction. However, pure BSA additive resulted in slightly opaque fibers, which was not observed with MC/Au@BSA, probably due to the more limited freedom and constrained structure of AuNC bound BSA. The MC/CNC-Au@GSH 3.0/0.75 and MC/Au@GSH 3.0/0.04 fibers were opaque and enough light could not pass through to measure the attenuation coefficients.

The mechanically strongest MC/CNC fibers at all three tested compositions (1.0/0.25, 2.0/0.50 and 3.0/0.75 yielded α in the range of 3.95 -5.39 dB cm^{-1}. Similar to the trend with pure MC fibers, also here thicker fibers yielded higher attenuation coefficients (Figure S17, Supporting Information). Thus, the fiber thickness controlled by the total solid content also correlated with the observed attenuation coefficient. Even though the α of MC/CNC fibers shows higher optical loss than pure MC fibers, it can still be considered relatively good among biopolymeric optical fibers in general. Remarkably, composite fibers prepared from MC/CNC/Au@BSA of 3.0/0.375/0.375 and 3.0/0.73/0.02 showed an attenuation coefficient of 3.5 dB cm^{-1} and 2.95 dB cm^{-1}, respectively. Importantly, these fibers also possess mechanical properties close to those of MC/CNC. Therefore, mechanically strong and ductile optical fibers with complementary properties are achieved.

Stretching of cellulosic fibers as a post-spinning processing method is known to align and reinforce the fiber structure, and it was probed here if the stretching would also affect the

optical signal attenuation.[90,91] Thus, MC 3.0 and MC/CNC 3.0/0.75 fiber samples were gently stretched to ca. 10%, after which the attenuation was measured. The attenuation coefficient of the stretched MC/CNC 3.0/0.75 fiber decreased from 5.39 to 4.34 dB cm^{-1} and is close to that of MC/Au@BSA 3.0/0.75 fibers. In contrast, practically no difference was observed with the MC 3.0, whose α remained at ~1.47 dB cm^{-1}. It is suggested that the stretching improved the alignment of CNCs inside MC/CNC fiber and mitigated the inherent defects in nanorod alignment originating, e.g., from the fiber flattening during the coagulation phase. Thus, stretching resulted in a more aligned structure, less scattering and improved signal transportation were achieved. In MC 3.0 fiber, the stretching effect remained negligible. The fiber did not contain larger rigid scattering objects similar to CNCs, i.e., the stretching of inherently homogeneous amorphous MC matrix did not produce as significant comparable overall structural changes.

2.6 Photostability and Metal Ion Sensing of MC-Gold Nanocluster Composite Fibers

Since gold nanoclusters were added to the MC fibers through a simple mixing procedure without disrupting their structure, their inherent characteristic properties, such as intense fluorescence, were retained and effectively transferred to the nanocomposite fibers. When MC/Au@BSA was exposed for continuous UV-irradiation at 365 nm for 12 h, significantly lower photoluminescence bleaching was observed than the Au@BSA. Thus, the incorporation of Au@BSA into the MC matrix allowed improved photostability. A similar trend was also noticed for Au@GSH and MC/Au@GSH. The Au@BSA is known to undergo fluorescence quenching in the presence of heavy metal ions, especially Hg^{2+}. To demonstrate whether the sensing abilities of Au@BSA was retained after fiber extrusion and drying, the nanocomposite fibers were studied for Hg^{2+} sensing using MC/Au@BSA 3.0/1.0, having slightly increased Au@BSA content for additional sensitivity (Figures 8 and Figure S18, Supporting Information).[70] The detection limit was found to be in the range of 1-10 mM upon fiber

immersion in Hg^{2+} containing solution qualitatively detected as quenching of the photoluminescence under UV light within a few minutes (Figure S18, Supporting Information).

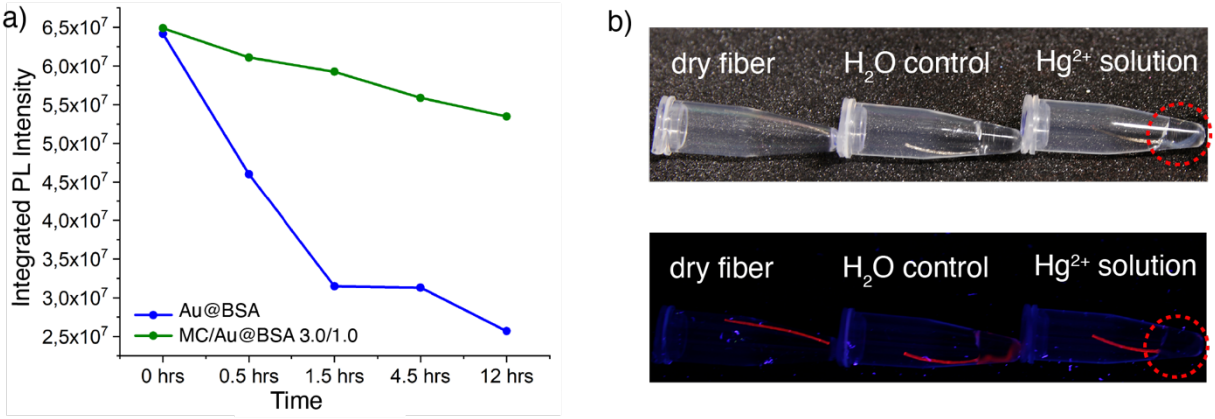

Figure 8. Photostability and metal ion sensing. a) Shows the integrated PL intensity as a function of time for Au@BSA (blue) and MC/Au@BSA (green) composite. b) Photographs showing mercury ion detection with MC/Au@BSA 3.0/1.0 fibers, left to right: dry control sample, fiber half-immersed in water, and fiber partly immersed in 10 mM aqueous Hg^{2+} solution (marked with a red circle) under ambient light (top) and UV-light (bottom).

2.7 Fiber Degradability under Aqueous Environment

The low optical loss and core-only nature of MC-based optical fibers would be well suited for biomedical applications where the required light propagation in tissue and organ-scale is tens of centimeters. Additionally, it is vital for components inserted into living tissues to be degradable in a reasonable time scale to avoid unnecessary surgical removal operations and tissue damage. We studied the preliminary degradation behavior of MC-based optical fibers under an aqueous environment at two different temperatures. Accordingly, MC/CNC 2.0/0.5 fibers were fixed at two ends using carbon tape inside a petri dish and subsequently added deionized water, maintaining the temperature at either 22 °C or 37 °C. The wetting and appearance of the fibers were then followed until complete disintegration or for a time period of 6 hours (Figure S19, Supporting Information). The fibers immersed in water at 22 °C completely degraded within 4 hours, showing highly hygroscopic behavior, which initially manifested as a rapid reversion to a more gel-like state. On the other hand, the fibers immersed in 37 °C survived substantially longer due to the LCST behavior of MC, which promotes

gelation and increased stiffness through the formation of stiff fibrillar aggregates at temperatures close to and above 40 °C.[60] Even though some structural softening and fiber elongation were observed, the fiber diameter remained relatively constant at 37 °C and the structural changes appeared to equilibrate into a stable hydrogel fiber. Moreover, the fibers could be picked up from the petri dish without breaking, suggesting highly persisting structural intactness and strength regardless of the extreme humidity and wetting. This encourages the search for potential application targets in biological or other environments with elevated or tunable temperatures.

3. Conclusions

In summary, MC-based optical fibers studied in this work are competitive among the known biopolymeric optical waveguides. The MC matrix offers ample opportunity to incorporate various dopants under ambient conditions. The low attenuation coefficient of MC-based optical fibers, tunable mechanical and optical properties, and high photostability offers complimentary multifunctional fibers. The Au@BSA and Au@GSH additives provided mechanical reinforcement of solid fibers at surprisingly low 0.04% contents and provided fibers with characteristic luminescence. Most importantly, the intrinsic optoelectronic properties and sensing capabilities of the gold nanoclusters were retained when incorporated into the MC matrix. At the same time, the composite fibers displayed high photostability against UV-irradiations. Thanks to the LCST characteristics of the MC matrix, fibers also showed temperature-dependent and tunable degradability in extreme wet conditions. The sustainable availability of cellulose, good mechanical and optical performance of the fibers, the scalability, and the simplicity of the fiber spinning process make the MC-based fibers a tempting material. The MC-based optical fibers pave the way for new, cellulose-based, and environmentally friendly composite optical materials. The observed mechanical characteristics are also in stark contrast to the standard silica glass optical fibers that have been reported to express maximum

stresses of ~1300 MPa (with polymer cladding) and 2600 MPa ("stripped" without cladding), the maximum strain of ~5% and 3%, and Young's moduli of 22 GPa and 83 GPa, respectively. The respective moduli of toughness estimated from the stress-strain graphs were 34 MJ m^{-3} and 33 MJ m^{-3}. Therefore, the maximum strain of the different MC-based fibers significantly surpassed the commercial silica optical fibers, while the modulus of toughness was roughly equal or higher. As a general difference, silica fibers show practically pure elastic behavior until breakage without noticeable yielding. In contrast, the MC-based fibers expressed a clear yield point after a relatively short elastic response followed by a significant plastic deformation region. This highlights the softness and ductility of the MC-based fibers compared to the silica optical fibers. For example, it is beneficial in biological and medical applications, where optical components should be flexible and match the surrounding tissue's dynamic mechanical properties and motion to avoid breaking the component itself or mechanically damaging its soft surroundings. In general, the relatively high RI of 1.48-1.50 of the MC-based nanocomposites is excellent for, e.g., applications in biological contexts, where the RI of biological tissues generally lie in the range of 1.38-1.41, i.e., favorable for efficient TIR.

EXPERIMENTAL SECTION

Materials and Reagents

Methylcellulose (MC, MW 88,000, product no. M0512), $HAuCl_4.3H_2O$, reduced glutathione (GSH), bovine serum albumin (BSA), sodium hydroxide, metal salts used in the metal ion sensing experiment and sulfuric acid used in the CNC synthesis were purchased from Sigma-Aldrich and used as received. Aqueous solvents prepared from acetate salts of sodium (Na^+), Potassium (K^+), lead (Pb^{2+}), cobalt (Co^{2+}), mercury (Hg^{2+}), magnesium (Mg^{2+}), nickel (Ni^{2+}), zinc (Zn^{2+}), chlorides of lithium (Li^+), calcium (Ca^{2+}), copper (Cu^{2+}) and iron (Fe^{3+}), and nitrates of cadmium (Cd^{2+}) and aluminum (Al^{3+}) were used to screen specific ionic sensitivity of MC/Au@BSA nanocomposite fibers. Whatman® 1 and Whatman® 541 filter papers and

Spectra/Por® 1 standard dialysis tubing (MW cut-off 6 – 8 kDa) used in the CNC preparation were purchased from VWR. Absolute ethanol (99.7 vol/vol-% Etax Aa, Altia Inc.) was used in the coagulation bath (diluted to 96.0% v/v) during fiber spinning. Ultrapure MilliQ® water (18 Ω) was used in all experiments.

Synthesis of BSA Encapsulated Gold Nanoclusters (Au@BSA)

The synthesis of Au@BSA was carried out following the reported procedure in the literature by Xie et al.[92] Briefly, 5 mL of 10 mM $HAuCl_4.3H_2O$ aqueous solution and 5 mL of aqueous BSA (50 mg/mL) solutions were prepared by dispersing in Milli Q (18 Ω) water and stored at 37 °C for 30 minutes. The aqueous solution of $HAuCl_4.3H_2O$ was then added to BSA solution under vigorous stirring at 37 °C. After 2 minutes, an aqueous solution of NaOH (1 M, 100 µL) was added to the above reaction mixture with constant stirring. A bright red dispersion of Au@BSA was produced within 12 hours of the reaction at 37 °C. Finally, the solution was cooled at room temperature and stored at 4 °C for further use.

Synthesis of GSH Functionalized Gold Nanoclusters (Au@GSH)

The synthesis of Au@GSH was performed according to a reported procedure by Luo et al.[93] Briefly, 500 µL (20 mM) of aqueous $HAuCl_4.3H_2O$ solution and 150 µL (100 mM) aqueous solution of glutathione were simultaneously added to 4.35 mL of Milli Q (18 Ω) water at 25 °C with gentle stirring over a magnetic stirrer. The stirring was continued for another 15 minutes until a colorless solution was obtained. The reaction mixture was heated at 70 °C for 24 hours in an oil bath with constant stirring of 500 rpm. Finally, the solution was cooled at room temperature and stored at 4 °C.

Synthesis of Gold Nanoclusters Covalently Linked to Cellulose Nanocrystals (CNC-Au@GSH)

In a typical synthesis, 500 µL (20 mM) aqueous solution of $HAuCl_4.3H_2O$ was mixed with 4.35 mL (14.5 mg/mL) of aqueous CNC dispersion with gentle stirring. The stirring was continued for 1 hour to allow the absorption of Au^{3+} over the negatively charged surface of CNC. To the reaction mixture, 150 µL (100 mM) aqueous solution of glutathione was added and the stirring was continued for another 15 minutes, followed by stirring at 70 °C for 24 hours. Finally, the solution was cooled to room temperature and the product was isolated by centrifugation at 4500 rpm for 3 hours. The supernatant was discarded and the CNC-Au@GSH residue was immediately mixed with 5 mL of water followed by vertexing to obtain colloidal dispersion. Finally, the dispersion was stored at 4 °C for further use.

Preparation of Cellulose Nanocrystals (CNCs)

The cellulose nanocrystals (CNCs) were prepared from cotton filter paper (Whatman® 1) *via* acid hydrolysis according to a previously reported procedure.[93] In brief, mechanically ground filter paper powder (15 g) was hydrolyzed with sulfuric acid (64 %, 300 mL) under gentle agitation at 45 °C for 45 min. The reaction was quenched by diluting 10-fold with MQ H_2O and sedimented overnight, after which the clear supernatant was discarded. The remaining dispersion was washed with two centrifugation – pellet re-dispersion cycles followed by dialysis against MQ H_2O until the conductivity of the dialysate remained below 5 µS cm^{-1}, and finally, a filtrated through Whatman® 541 filter paper. The ready-made CNCs were stored at + 4 °C until use. The solid content was determined gravimetrically, and the material was characterized by TEM, dynamic light scattering (DLS), zeta (ζ) potential measurements, and conductometric titration (Figure S1). Characterization data and experimental details are presented in the Supporting Information.

Preparation of Methylcellulose and Methylcellulose-Nanocomposite Hydrogels

The desired amount of dry MC powder was dissolved in hot (~85 °C) MQ water according to the supplier's instructions and vigorously stirred until a homogeneous cloudy solution was achieved. The solution was cooled down in a cold water bath (~10 °C) under constant mild shaking to hydrate the MC polymer chains and to promote even gelation until the material turned fully clear and transparent indicative of the gel state. Ready-made gels were stored at +4 °C until use. 2.0 % (w/v = 20 mg/mL), 3.0% and 4.0% pure MC gels were prepared. Gold nanoclusters, CNC-Au@GSH and CNC dopants were pre-heated and added into the hot MC solution prior to the gelation, when needed, to guarantee homogeneous particle distribution within the gels. Gels relied fully on weak physical interactions of the components. MC-Bovine serum albumin control samples (without gold clusters) were prepared by mixing MC powder into pre-made and pre-heated BSA solution. Typically, MC composites with a final concentration of 3.0% of MC and 0.75% of a dopant were prepared to allow comparison based on the materials' total solid content. The gels were characterized with oscillatory rheological measurements and used for wet spinning of solid optical fibers. Furthermore, gels were used to prepare thin films for supportive optical and structural characterization of the bulk material. The details, including the characterization methods, are reported in the Supporting Information.

Fiber Spinning and Characterization

MC-based hydrogels were wet-spun into solid fibers by extrusion (1.8 mL/min constant flow speed) through a thin capillary tube (ø = 1 mm, length = 1 m) into a coagulation bath filled with ethanol (96.0 v/v-%) at room temperature (~22 °C).[85] The extrusion setup is schematically depicted in Figure 1. Before the extrusion, the gels were centrifuged (3000 rpm, 1-3 min) to remove possible gel-trapped air bubbles. The extrusion capillary was guided by hand so that the freshly extruded fiber did not overlap itself in the coagulation bath in order to avoid merging of the wet fiber segments. The selected flow speed allowed comfortable manual maneuverability while remaining fast enough to produce good quality fibers. The nascent fiber

was allowed to coagulate in ethanol for at least 25 min after which it was cut into ~8 cm long sample pieces and suspended to dry vertically fixed at both ends at ambient conditions (~22 °C, >15 h). The fibers are labeled and discussed in the text according to their initial hydrogel percentage (w/v) compositions. For example, MC 2.0 fiber has been spun from 2.0% (i.e., 20 mg/mL) MC aq. dispersion.

The mechanical properties of the fibers were studied by uniaxial tensile tests using a 5 kN tensile/compression module (Kammrath & Weiss GMbH, Germany) fitted with a 100 N load cell. The morphology and structure of the fibers were imaged with light microscopy and scanning electron microscopy (SEM). Degradation tests were used to study the durability of the fibers in various conditions. The experimental details on tensile tests, microscopy and degradation experiments are given in the Supporting Information.

To investigate the light-guiding properties of the fibers, the cutback method was used to assess the attenuation coefficients (α) of the fibers with different compositions following a reported literature procedure.[33]

Supporting Information

Supporting Information is available from the Wiley Online Library or the authors.

Acknowledgments

V. H and S.C. contributed equally to this work. This work was carried out under the Academy of Finland´s Centre of Excellence in Molecular Engineering of Biosynthetic Hybrid Materials Research (HYBER, 2014-2019), ERC for Advanced grant (Driven 2017-2022), FinnCERES, and Photonic Research and Innovation (PREIN) Flagship (Grant No. 320167). Z.S. acknowledges funding from the Academy of Finland (Grant Nos. 325810, 312297, and 314810) and ERC grant (Grant No. 834742). S. C. acknowledges the Academy of Finland for project funding (Grant No. 310799). We acknowledge the provision of facilities and technical support

by Aalto University OtaNano – Nanomicroscopy Center (Aalto-NMC). P.M. acknowledges the Jenny and Antti Wihuri Foundation (Centre for Young Synbio Scientists). V.H. acknowledges financial support from Walter Ahlström Foundation and Finnish Foundation for Technology Promotion. We thank the doctoral candidate M. Junaid for useful discussions related to surface characterization.

Received: ((will be filled in by the editorial staff))
Revised: ((will be filled in by the editorial staff))
Published online: ((will be filled in by the editorial staff))

References

[1] J. Hecht, *City of Light: The Story of Fiber Optics* (Oxford University Press, New York, 2004)

[2] Z. Liu, Z. F. Zhang, H.-Y. Tam, X. Tao, *Photonics* **2019**, *6*, 48.

[3] D. Shan, E. Gerhard, C. Zhang, J. W. Tierney, D. Xie, Z. Liu, J. Yang, *Bioactive Mater.* **2018**, *3*, 434.

[4] Y. Koike, M. Asai, *NPG Asia Mater*. **2009**, *1*, 22–28.

[5] H. Ma, A. K.-Y. Jen, L. R. Dalton, *Adv. Mater.* **2002**, *14*, 1339.

[6] J. Böhm, J. Haußelt, P. Henzi, K. Litfin, T. Hanemann, *Adv. Eng. Mater.* **2004**, *6*, 52.

[7] K. Peters, *Smart Mater. Struct.* **2011**, *20*, 013002.

[8] P. Wang, Y. Wang, L. Tong, *Light Sci. and Appl.* **2013**, *2*, 102.

[9] A. Camposeo, F. di Benedetto, R. Stabile, A. A. R. Neves, R. Cingolani, D. Pisignano, *Small* **2009**, *5*, 562.

[10] J. Chen, P. Yang, C. Wang, S. Zhan, L. Zhang, Z. Huang, W. Li, C. Wang, Z. Jiang, C. Shao, *Nanoscale Res. Lett.* **2011**, *6*, 121.

[11] H. Liu, J. B. Edel, L. M. Bellan, H. G. Craighead, *Small* **2006**, *2*, 495.

[12] C. Grivas, J. Yang, M. B. J. Diemeer, A. Driessen, M. Pollnau, *Opt. Lett.* **2010**, *35*, 1983.

[13] M. Lu, H. Zhu, C. G. Bazuin, W. Peng, J. F. Masson, *ACS Sensors* **2019**, *4*, 613.

[14] J. Guo, B. Zhou, C. Yang, Q. Dai, L. Kong, *Adv. Funct. Mater.* **2019**, *29*, 1902898.

[15] M. Lanzarini-Lopes, B. Cruz, S. Garcia-Segura, A. Alum, M. Abbaszadegan, P. Westerhoff, *Environ. Sci. Technol.* **2019**, *53*, 10880.

[16] Nonappa, *Beilstein J. Nanotechnol.* **2020**, *11*, 533.

[17] J. B. Li, H. W. Liu, T. Fu, R. Wang, X. B. Zhang, W. Tan, *Trends Chem.* **2019**, *1*, 224.

[18] C. P. Montgomery, B. S. Murray, E. J. New, R. Pal, D. Parker, *Acc. Chem. Res.* **2009**, *42*, 925.

[19] U. Resch-Genger, M. Grabolle, S. Cavaliere-Jaricot, R. Nitschke, T. Nann, *Nat. Methods* **2008**, *5*, 763.

[20] M. Montalti, A. Cantelli, G. Battistelli, *Chem. Soc. Rev.* **2015**, *44*, 4853.

[21] A. Lacraz, M. Polis, A. Theodosiou, C. Koutsides, K. Kalli, *IEEE Photonics Technol. Lett.* **2015**, *27*, 693.

[22] D. L. Kaplan, R. Hartenstein, J. Sutter, *Appl. Environ. Microbiol.* **1979**, *38*, 551.

[23] M. C. J. Large, J. Moran, L. Ye, *Meas. Sci. Technol.* **2009**, *20*, 034014.

[24] K. Makino, Y. Akimoto, K. Koike, A. Kondo, A. Inoue, Y. Koike, *J. Light. Technol.* **2013**, *31*, 2407.

[25] A. Jain, A. H. J. Yang, D. Erickson, *Opt. Lett.* **2012**, *37*, 1472.

[26] M. Choi, M. Humar, S. Kim, S.-H. Yun, *Adv. Mater.* **2015**, *27*, 4081.

[27] J. Guo, X. Liu, N. Jiang, A. K. Yetisen, H. Yuk, C. Yang, A. Khademhosseini, X. Zhao, S.-H. Yun, *Adv. Mater.* **2016**, *28*, 10244.

[28] N. Jiang, R. Ahmed, A. A. Rifat, J. Guo, Y. Yin, Y. Montelongo, H. Butt, A. K. Yetisen, *Adv. Opt. Mater.* **2018**, *6*, 1701118.

[29] R. T. Chen, W. Phillips, T. Jannson, D. Pelka, *Opt. Lett.* **1989**, *14*, 892.

[30] A. K. Manocchi, P. Domachuk, F. G. Omenetto, H. Yi, *Biotechnol. Bioeng.* **2009**, *103*, 725.

[31] L. H. Chen, T. Li, C. C. Chan, R. Menon, P. Balamurali, M. Shaillender, B. Neu, X. M. Ang, P. Zu, W. C. Wong, K. C. Leong, *Sens. Actuators B Chem.* **2012**, *169*, 167.

[32] S. S. Voznesenskiy, A. A. Sergeev, A. Yu. Mironenko, S. Yu. Bratskaya, Yu. N. Kulchin, *Sens. Actuators B Chem.* **2013**, *188*, 482.

[33] A. Yu. Mironenko, A. A. Sergeev, A. E. Nazirov, E. B. Modin, S. S. Voznesenskiy, S. Yu. Bratskaya, *Sens. Actuators B Chem.* **2016**, *225*, 348.

[34] F. G. Omenetto, D. L. Kaplan, *Nat. Photonics* **2008**, *2*, 641.

[35] S. T. Parker, P. Domachuk, J. Amsden, J. Bressner, J. A. Lewis, D. L. Kaplan, F. G. Omenetto, *Adv. Mater.* **2009**, *21*, 2411.

[36] H. Tao, J. M. Kainerstorfer, S. M. Siebert, E. M. Pritchard, A. Sassaroli, B. J. B. Panilaitis, M. A. Brenckle, J. J. Amsden, J. Levitt, S. Fantini, D. L. Kaplan, F. G. Omenetto, *Proc. Natl. Acad. Sci.* **2012**, *109*, 19584.

[37] S. Kujala, A. Mannila, L. Karvonen, K. Kieu, Z. Sun, *Sci. Rep.* **2016**, *6*, 22358.

[38] S. Nizamoglu, M. C. Gather, M. Humar, M. Choi, S. Kim, K. S. Kim, S. K. Hahn, G. Scarcelli, M. Randolph, R. W. Redmond, S. H. Yun, *Nat. Commun.* **2016**, *7*, 10374.

[39] E. M. Heckman, J. G. Grote, F. K. Hopkins, P. P. Yaney, *Appl. Phys. Lett.* **2006**, *89*, 181116.

[40] W. Jung, B. Paulson, K. Choi, J. Y. Son, T. Nazari, S. H. Park, J. H. Kim, K. Oh, in *Optical Processes in Organic Materials and Nanostructures II* (Eds: M. Eich, J.-M. Nunzi, R. Jakubiak), Proc. SPIE 8827, **2013**.

[41] D. Klemm, B. Heublein, H.-P. Fink, A. Bohn, *Angew. Chem. Intl. Ed.* **2005**, *44*, 3358

[42] D. Li, L. Wang, *Opt. Commun.* **2010**, *283*, 2841.

[43] L. Peng, X. Yang, L. Yuan, L. Wang, E. Zhao, F. Tian, Y. Liu, *Opt. Commun.* **2011**, *284*, 4810.

[44] A. Lokman, S. Nodehi, M. Batumalay, H. Arof, H. Ahmad, S. W. Harun, *Microw. Opt. Technol. Lett.* **2014**, *56*, 380.

[45] A. Espinha, G. Guidetti, M. C. Serrano, B. Frka-Petesic, A. G. Dumanli, W. Y. Hamad, Á. Blanco, C. López, S. Vignolini, *ACS Appl. Mater. Interfaces* **2016**, *8*, 31935.

[46] G. Guidetti, S. Atifi, S. Vignolini, W. Y. Hamad, *Adv. Mater.* **2016**, *28*, 10042.

[47] F. I. Chowdhury, C. Dick, L. Meng, S. M. Mahpeykar, B. Ahvazi, X. Wang, *RSC Adv.* **2017**, *7*, 32436.

[48] B. Frka-Petesic, G. Guidetti, G. Kamita, S. Vignolini, *Adv. Mater.* **2017**, *29*, 1701469.

[49] Y.-D. He, Z.-L. Zhang, J. Xue, X.-H. Wang, F. Song, X.-L. Wang, L.-L. Zhu, Y.-Z. Wang, *ACS Appl. Mater. Interfaces* **2018**, *10*, 5805.

[50] M. S. Toivonen, O. D. Onelli, G. Jacucci, V. Lovikka, O. J. Rojas, O. Ikkala, S. Vignolini, *Adv. Mater.* **2018**, *30*, 1704050.

[51] O. Kose, A. Tran, L. Lewis, W. Y. Hamad, M. J. MacLachlan, *Nat. Commun.* **2019**, *10*, 510.

[52] T. H. Zhao, R. M. Parker, C. A. Williams, K. T. P. Lim, B. Frka-Petesic, S. Vignolini, *Adv. Funct. Mater.* **2019**, *29*, 1804531.

[53] E. Kontturi, P. Laaksonen, M. B. Linder, Nonappa, A. H. Gröschel, O. J. Rojas, O. Ikkala, *Adv. Mater*. **2018**, *30*, 1703779.

[54] K. Heise, E. Kontturi, Y. Allahverdiyeva, T. Tammelin, M. B. Linder, Nonappa, O. Ikkala, *Adv. Mater.* **2020**, 2004349 (DOI: 10.1002/adma.202004349).

[55] A. Dupuis, N. Guo, Y. Gao, N. Godbout, S. Lacroix, C. Dubois, M. Skorobogatiy, *Opt. Lett.* **2007**, *32*, 109.

[56] H. Orelma, A. Hokkanen, I. Leppänen, K. Kammiovirta, M. Kapulainen, A. Harlin, *Cellulose* **2020**, 27. 1543.

[57] T. L. Rogers, D. Wallick, *Drug Dev. Ind. Pharm.* **2012**, *38*, 129.

[58] P. L. Nasatto, F. Pignon, J. L. M. Silveira, M. E. R. Duarte, M. D. Noseda, M. Rinaudo, *Polymers* **2015**, *7*, 777.

[59] H. C. Arca, L. I. Mosquera-Giraldo, V. Bi, D. Xu, L. S. Taylor, K. J. Edgar, *Biomacromolecules* **2018**, *19*, 2351.

[60] L. Li, *Macromolecules* **2002**, *35*, 5990.

[61] J. P. A. Fairclough, H. Yu, O. Kelly, A. J. Ryan, R. L. Sammler, M. Radler, *Langmuir* **2012**, *28*, 10551.

[62] S. A. Arvidson, J. R. Lott, J. W. McAllister, J. Zhang, F. S. Bates, T. P. Lodge, R. L. Sammler, Y. Li, M. Brackhagen, *Macromolecules* **2013**, *46*, 300.

[63] J. V. Rie, W. Thielemans, *Nanoscale*, **2017**,*9*, 8525.

[64] R. Jin, C. Zeng, M. Zhou, Y. Chen, *Chem. Rev.* **2016**, *116*, 10346.

[65] I. Chakraborty, T. Pradeep, *Chem. Rev.* **2017**, *117*, 8208.

[66] J. V. Rival, P. Mymoona, K. M. Lakshmi, Nonappa, T. Pradeep, E. S. Shibu, *Small* **2020**, 2005718 (DOI:10.1002/smll.202005718)

[67] Nonappa, T. Lahtinen, Johannes. S. Haataja, T.-R. Tero, H. Häkkinen, O. Ikkala, *Angew. Chem. Intl. Ed.* **2016**, *55*, 16035.

[68] Nonappa, O. Ikkala, *Adv. Funct. Mater.***2018**, *28*, 1704328.

[69] L. Zhang, E. Wang, *Nano Today* **2014**, *9*, 132.

[70] N. Mohammed, A. Baidya, V. Murugesan, A. A. Kumar, M. A. Ganayee, J. S. Mohanty, K. C. Tam, T. Pradeep, *ACS Sustain. Chem. Eng.* **2016**, *4*, 6167.

[71] A. Senthamizhan, A. Celebioglu, T. Uyar, *J. Mater. Chem. A* **2014**, *2*, 12717.

[72] U. S. Akshath, P. Bhatt, S. A. Singh, *J. Fluoresc.* **2020**, *30*, 537.

[73] K. Chaudhari, P. L. Xavier, T. Pradeep, *ACS Nano* **2011**, *5*, 8816.

[74] G. Li, R. Jin, *Acc. Chem. Res.* **2013**, *46*, 1749.

[75] Y. S. Chen, P. V. Kamat, *J. Am. Chem. Soc.* **2014**, *136*, 6075.

[76] S. Chandra, Nonappa, G. Beaune, A. Som, S. Zhou, J. Lahtinen, H. Jiang, J. V. I. Timonen, O. Ikkala, R. H. A. Ras, *Adv. Opt. Mater.* **2019**, *7*, 1900620.

[77] S. H. Yau, O. Varnavski, T. Goodson, *Acc. Chem. Res.* **2013**,*46*, 1506.

[78] Y. Z. Lu, W. Chen W. *Chem. Soc. Rev.* **2012**, *41*, 3594.

[79] N. Goswami, F. Lin, Y. Liu, D. T. Leong, J. Xie, *Chem. Mater*. **2016**, *28*, 4009.

[80] K. Pyo, V. D. Thanthirige, K. Kwak, P. Pandurangan, G. Ramakrishna, D. Leev, *J. Am. Chem. Soc.* **2015**, *137*, 25, 8244.

[81] X. Kang, M. Zhu, *Chem. Soc. Rev*. **2019**, *48*, 2422.

[82] K. Chaudhari, P. L. Xavier, T. Pradeep *ACS Nano* **2011**, *5*, 11, 8816.

[83] P. L. Xavier, K. Chaudhari, A. Baksi, T. Pradeep, *Nano Rev.* **2012**, *3*, 14767.

[84] V. Hynninen, S. Hietala, J. R. McKee, L. Murtomäki, O. J. Rojas, O. Ikkala, Nonappa, *Biomacromolecules* **2018**, *19*, 2795.

[85] V. Hynninen, P. Mohammadi, W. Wagermaier, S. Hietala, M. B. Linder, O. Ikkala, Nonappa, *Eur. Polym. J.* **2019**, *112*, 334.

[86] P. Mohammadi, M. S. Toivonen, O. Ikkala, W. Wagermaier, M. B. Linder, *Sci. Rep.* **2017**, *7*, 11860.

[87] S. C. Baxter, C. T. Robinson, *Compos. Sci. Technol.* **2011**, *71*, 1273.

[88] A. Pakzad, J. Simonsen, R. S. Yassar, *Compos. Sci. Technol.* **2012**, *72*, 314.

[89] J. Sapkota, J. C. Martinez Garcia, M. Lattuada, *J. Appl. Polym. Sci.* **2017**, *134*, 45254.

[90] J. G. Torres-Rendon, F. H. Schacher, S. Ifuku, A. Walther, *Biomacromolecules* **2014**, *15*, 2709.

[91] H. C. Kim, D. Kim, J. Y. Lee, L. Zhai, J. Kim, *Int. J. Precis. Eng. Manuf. Green Tech.* **2019**, *6*, 567.

[92] J. Xie, Y. Zheng, J. Y. Ying, *J. Am. Chem. Soc.* **2009**, *131*, 888.

[93] Z. Luo, X. Yuan, Y. Yu, Q. Zhang, D. T. Leong, J. Y. Lee, J. Xie, *J. Am. Chem. Soc.* **2012**, *134*, 16662.

Table of content entry

V. Hynninen, S. Chandra, S. Das, M. Amini, Y. Dai, S. Lepikko, P. Mohammadi, S. Hietala, R. H. A. Ras, Z. Sun, O. Ikkala*, Nonappa*

Luminescent Gold Nanocluster-Methylcellulose Composite Optical Fibers with Low Attenuation Coefficient and High Photostability

Simple extrusion of shear-thinning aqueous methylcellulose dispersions and its composite hydrogels with gold nanoclusters, cellulose nanocrystals, or cellulose nanocrystal-gold nanocluster hybrids enables mechanically and optically tunable biopolymeric optical fibers. The resulting strong and ductile composite fibers display low attenuation coefficient making them suitable for application in short-distance optical fibers.